GEOLOGY

The largest deep-ocean silicic volcanic eruption of the past century

Rebecca Carey,[1]* S. Adam Soule,[2] Michael Manga,[3] James D. L. White,[4] Jocelyn McPhie,[1] Richard Wysoczanski,[5] Martin Jutzeler,[1] Kenichiro Tani,[6] Dana Yoerger,[2] Daniel Fornari,[2] Fabio Caratori-Tontini,[7] Bruce Houghton,[8] Samuel Mitchell,[8] Fumihiko Ikegami,[1] Chris Conway,[6] Arran Murch,[4] Kristen Fauria,[3] Meghan Jones,[2,9] Ryan Cahalan,[10] Warren McKenzie[8]

The 2012 submarine eruption of Havre volcano in the Kermadec arc, New Zealand, is the largest deep-ocean eruption in history and one of very few recorded submarine eruptions involving rhyolite magma. It was recognized from a gigantic 400-km² pumice raft seen in satellite imagery, but the complexity of this event was concealed beneath the sea surface. Mapping, observations, and sampling by submersibles have provided an exceptionally high fidelity record of the seafloor products, which included lava sourced from 14 vents at water depths of 900 to 1220 m, and fragmental deposits including giant pumice clasts up to 9 m in diameter. Most (>75%) of the total erupted volume was partitioned into the pumice raft and transported far from the volcano. The geological record on submarine volcanic edifices in volcanic arcs does not faithfully archive eruption size or magma production.

INTRODUCTION

Volcanism within the ocean basins currently comprises 70% of Earth's magma output (1, 2), but submarine eruptions are not as well understood as their on-land counterparts because of the challenges in both directly observing eruptions and accessing deposits (3). Recent observations of explosive and effusive submarine eruptions in the Tonga and Marianas volcanic arcs have driven a surge in understanding deep, low-intensity, mafic end-member eruption styles (4–6). In contrast, the behavior of deep silicic eruptions in submarine settings is much less well known. Our understanding of deep silicic submarine eruptions is based largely on studying uplifted ancient successions, where details are limited by restricted exposures and missing context such as knowledge of timing and duration, source vents, and water depths (3, 7). Direct insights are possible from modern seafloor deposits (8–11), but observational records of silicic submarine eruptions are rare (12–15), duration and timing information are not available, and there are no examples where the products of a large submarine silicic eruption have been mapped and characterized shortly after eruption.

In 2012, a ~400-km² pumice raft was observed and tracked to Havre caldera volcano in the Kermadec arc. The size of the raft indicated that it was produced by the largest deep-water (>500 m below sea level) silicic submarine eruption ever recorded (Fig. 1 and fig. S1) (16, 17). Seafloor bathymetry of Havre volcano collected before and after eruption in 2002 and 2012 was conducted with R/V Tangaroa using an EM300 and EM302 shipboard multibeam echosounder (25-m resolution), respectively (17, 18). Bathymetry changes were attributed to the products of

explosive underwater eruptions from at least seven different vents based on apparent cone-like geometries and summit depressions (17).

RESULTS

The 2015 investigation of Havre volcano reported here included an EM122 shipboard multibeam survey along with an autonomous underwater vehicle (AUV) *Sentry* near-bottom multibeam survey of the entire Havre caldera and rim from which a comprehensive 1-m resolution bathymetric map was produced (Fig. 2 and figs. S2.1 and S2.2). The AUV survey overturned the previous interpretations, revealing in fine detail lavas and domes from 14 different vents, mass-wasting deposits, and dispersed seafloor pumice deposits. In parallel, and guided by the high-resolution AUV bathymetry, 12 remotely operated vehicle (ROV) dives of 250 hours total duration were executed. The dives provided photos and video footage of the seafloor and samples at 290 locations on the volcano and inside the caldera (fig. S2.3). All the lava and clastic products associated with this eruption are rhyolitic in composition (70 to 72 weight % SiO_2; table S1A).

The AUV bathymetric map and ROV seafloor investigations revealed a complex eruption history that was not apparent from the limited satellite observations of the ocean surface. The most conspicuous features resolved by the near-bottom bathymetry are large zones of contrasting rough and smooth terrains overprinting the regional morphology of the caldera floor and flanks (Fig. 2 and fig. S3). The rough terrain reflects the distribution of a continuous blanket of giant (1- to 9-m-diameter) pumice clasts [giant pumice (GP)] with a footprint of 35 km² in the mapped area (Figs. 2 and 3, A and B). Attempts to sample GP clasts revealed that they are delicate and easily shattered. Their precarious stacking up to four clasts high in places implies gentle settling from the water column. The sizes of pumice clasts in the seafloor deposit are very consistent, indicating a high degree of sorting; by visual estimate from recorded videos, >>95% by volume of all clasts observed are greater than 30 cm in diameter, including where the deposit is exposed in cross section or on its distal edges. The edge of the GP deposit on the bathymetric map is marked by the transition to a smooth seafloor, where >1 m–sized pumice clasts are absent (Fig. 2 and fig. S3). ROV observations of the GP deposit edges show that it becomes a

[1]CODES and School of Physical Sciences, University of Tasmania, Hobart, Tasmania 7001, Australia. [2]Woods Hole Oceanographic Institution, Woods Hole, MA 02543, USA. [3]Department of Earth and Planetary Science, University of California, Berkeley, 307 McCone Hall, Berkeley, CA 94720–4767, USA. [4]Geology Department, University of Otago, Dunedin 9054, New Zealand. [5]National Institute of Water and Atmospheric Research, Auckland, New Zealand. [6]Department of Geology and Paleontology, National Museum of Nature and Science, 4-1-1 Amakubo, Tsukuba-shi, Ibaraki 305-0005, Japan. [7]GNS Science, P.O. Box 30368, Lower Hutt 5010, New Zealand. [8]Geology and Geophysics, University of Hawaii at Manoa, 1680 East-West Road, Honolulu, HI 96825, USA. [9]Massachusetts Institute of Technology/Woods Hole Oceanographic Institution Joint Program in Oceanography/Applied Ocean Science and Engineering, Woods Hole, MA 02543, USA. [10]School of Earth and Atmospheric Sciences, Georgia Institute of Technology, 311 Ferst Drive, Atlanta, GA 30332, USA.
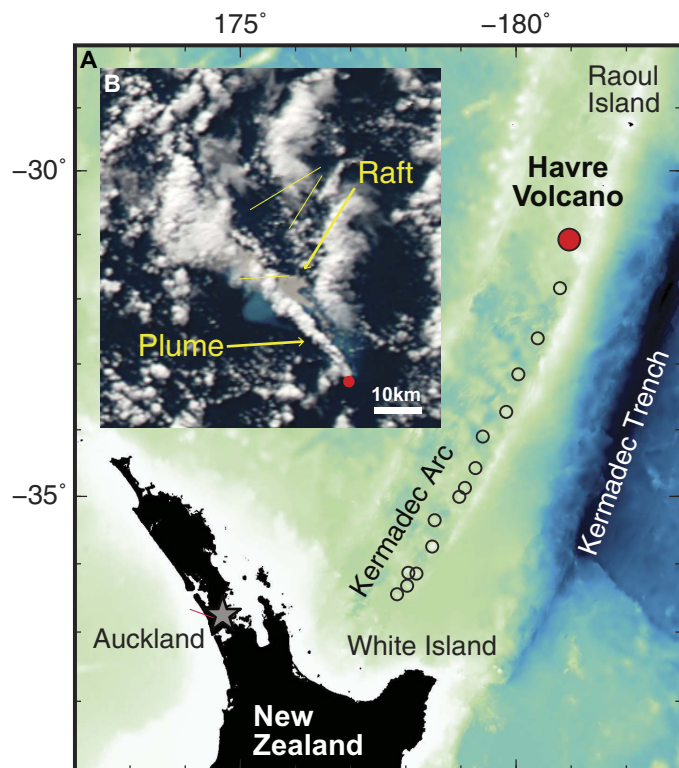*Corresponding author. Email: rebecca.carey@utas.edu.au

Fig. 1. Location map of Havre volcano and NASA MODIS satellite imagery. (A) Location map of Havre volcano in the Kermadec arc, New Zealand. Open dots are locations of Kermadec arc volcanoes to the south of Havre. (B) NASA Moderate Resolution Imaging Spectroradiometer (MODIS) satellite image taken at 01:26 UTC, 19 July 2012, ~21 hours after the onset of the pumice raft generation. A vapor plume is visible at the source of the raft; whether or not there were particles in the plume is unknown. The red dot is the location of Havre volcano.

discontinuous apron of coarse decimeter-to-meter–sized clasts. The GP clasts display curviplanar surfaces, commonly with normal joints, and breadcrust textures, suggesting that they formed by brittle fragmentation, involving quenching (Fig. 3C) (19, 20). The retrieval of a complete 1 m × 0.9 m × 0.7 m GP clast (GP290) and subsequent density analysis reveal modal external and internal values of 600 and 500 kg m^{-3}, respectively (movie S1 and fig. S4).

On the southwest side of the caldera, five lavas (A to E) were erupted at depths between 1220 and 1140 m; their vents are spaced between 50 and 380 m from one another (Fig. 2, in red). The eruption of lavas A to E on the steep caldera wall formed initial steep and narrow (<130 m) lava tongues that cause lavas A and C to spread into 30-m-high, 100- to 500-m-wide lava lobes on the caldera floor. The bathymetry also reveals a further nine vents that erupted lavas and domes along a segment of the southern caldera rim at depths of 1050 to 900 m (Fig. 2). The westernmost vents produced both lavas and domes (F to I; Fig. 2), the northern margins of which are steeply truncated along the caldera wall. Directly downslope from lavas G to I, chaotic, coarse deposits become finer toward the center of the caldera where they bury GP clasts on the caldera floor and lava C (MW in green; Fig. 2). We link this coarse deposit to submarine debris avalanches and associated debris flows formed by the collapse of lavas G to I. At the eastern end of the segment are four discrete lava domes (K to N) and a much larger dome complex on the southeastern point of the caldera rim (O-P).
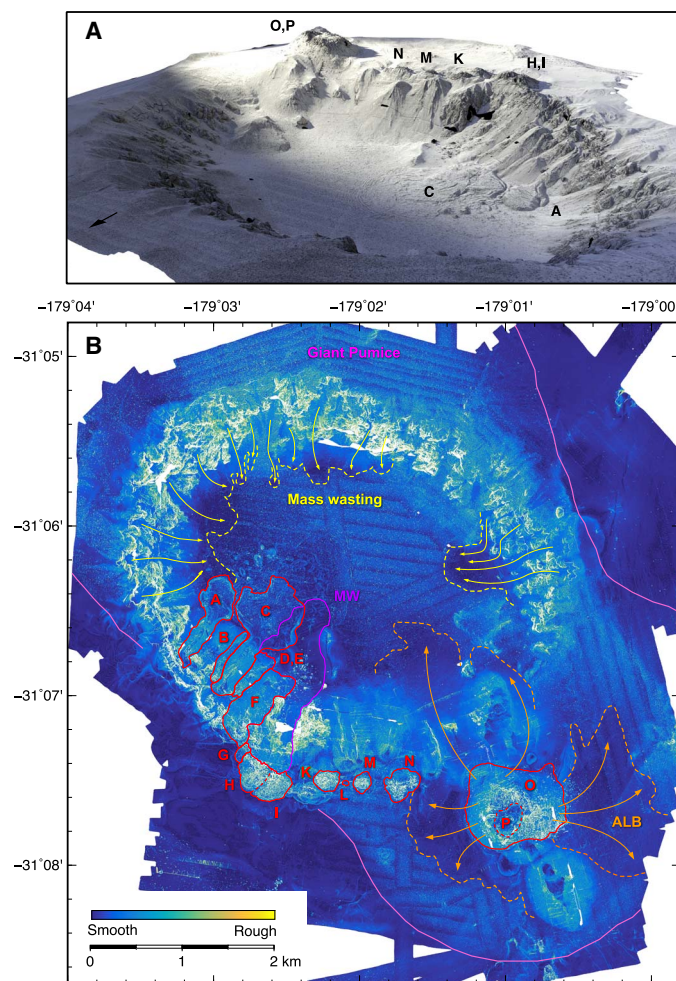

Fig. 2. Two-dimensional surface roughness map and three-dimensional rendering of Havre submarine volcano. (A) Three-dimensional surface rendering of the Havre submarine caldera, view looking from the northeast. Lavas distributed on the southern margin of the caldera are labeled [see (B)]. The width of the caldera is 4.5 km. (B) Seafloor roughness, derived from the gridded AUV bathymetry by calculating the surface area in 3 × 3 m bins relative to a flat seafloor. As expected, the steep caldera walls show high roughness. The lavas and domes (outlined in red and labeled A to P) are distinguished by high roughness. The sediment at the lava flow front of lava C is wrinkled. A coarse deposit interpreted as the product of syneruptive mass wasting is located within the caldera extends north-northeast from the truncated edges of lavas G to I (MW in red). The widespread GP deposit has moderate roughness on the caldera floor and flanks and is outlined by solid pink lines. Areas within the GP deposit that are less rough are partially or wholly buried by ALB, and later deposits are derived from the collapse of dome O-P (dashed orange lines). Dashed yellow lines enclose parts of the GP deposits covered by syn- and post-eruption mass-wasting deposits inside the caldera.

Two further pumice deposits were identified: (i) ash-lapilli-block (ALB) and (ii) ash-lapilli (AL) deposits (Fig. 3, E and F). The ALB deposit is a <0.01 km^3 (bulk) radially thinning blanket of ash to 1 m–sized pumice blocks up to 2 m thick and circumferentially dispersed to a distance of 2 km around, and extending beneath, the lava dome complex O-P (Figs. 2 and 3E and table S2). The AL deposit is a <0.1 km^3 (bulk) pumice deposit up to 40 cm thick comprising ash and subordinate fine lapilli, which is dispersed across the entire volcano summit (Fig. 3F and table S2).
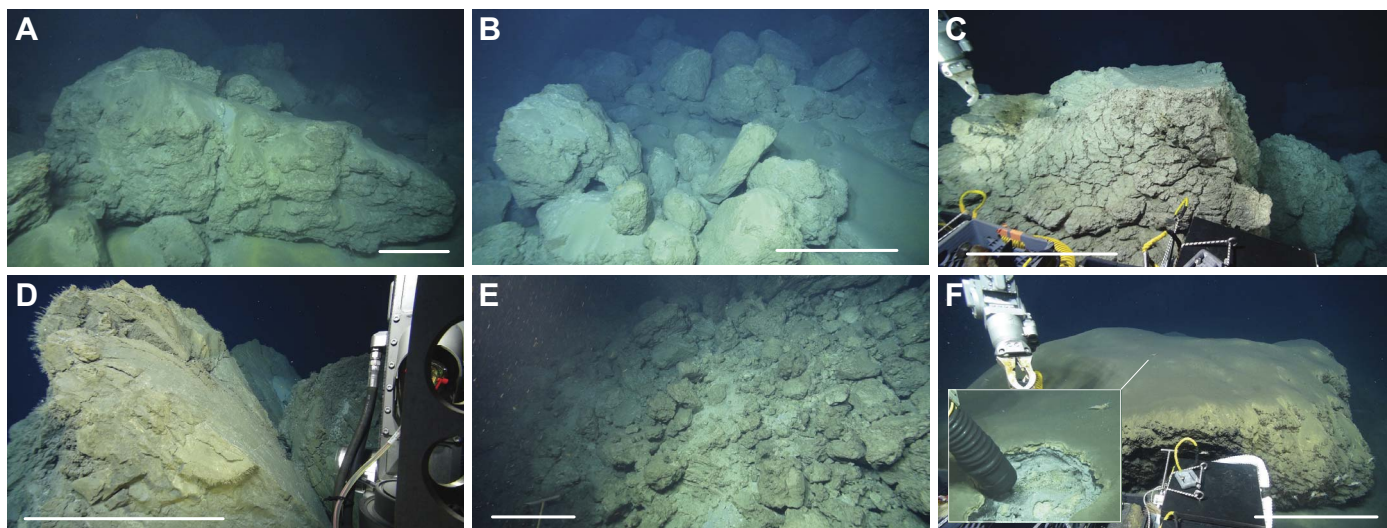
Fig. 3. Seafloor products of the 2012 Havre eruption. Images taken from the forward-looking ROV cameras of lava, domes, and clastic deposits. Line in each image is 1 m in length. (**A**) GP clasts are predominantly meter-sized; the clast shown here is 6 m in diameter. (**B**) Meter-sized GP clasts are stacked more than four clasts high within the caldera, suggesting gentle settling to the seafloor from suspension. (**C**) GP clasts commonly have curviplanar surfaces and quenched margins with normal joints and breadcrusting. (**D**) Lava spine on dome O-P. (**E**) ALB deposit at 1.2 km from the inferred source vent (dome O-P). (**F**) AL deposit on top of a GP clast; inset shows the complex internal stratigraphy of this unit.

Jutzeler *et al.* (*16*) calculated a minimum raft pumice volume of 0.11 to 0.16 km^3 (bulk). This estimate was based on the thickness (average, 50 to 70 cm) of the raft encountered 3 weeks after the eruption, and raft area (400 km^2) at 60% clast packing density. New additional observations of the raft revealed that it was 1 to 2 m thick 19 days after the eruption (*21*) and was made up of densely packed, stacked clasts up to 75 cm in diameter. We suggest that a raft thickness of 5 m is reasonable, implying a pumice raft bulk volume of 1.2 km^3. Shallow-water curtains of submerged pumice evident as 120-km^2 aqua blue regions on 18 to 19 July [coordinated universal time (UTC)] satellite imagery are not incorporated into our estimate and would increase the values of the erupted volume and mass (fig. S1). The details of the calculation and associated uncertainties are given in Materials and Methods.

On the seafloor, the GP deposit volumetrically dominates all other pumice deposits at 0.1 km^3 (bulk). The volume of the seafloor 2012 lavas and domes has been calculated using the 2002 pre-eruption (*18*) and the 2015 high-resolution bathymetry and thickness/dispersal observations (table S2). The 14 lavas and domes have an equivalent combined volume of 0.21 km^3 (dense rock equivalent), and dome O-P represents half of this erupted volume.

A detailed and valuable measure of eruption dynamics is the intensity, the mass, or the volume of magma discharged per unit time (*22*). This is a significant challenge in the submarine setting because duration has never been measured directly for a silicic submarine eruption. Satellite imagery of the Havre 2012 pumice raft allows us to place constraints on both volume and duration on this phase of the eruption. Assuming that the detachment of the raft from the point source and cessation of the plume (observed in MODIS images; fig. S1) marked the end of the eruption, most of the raft pumice volume (1.2 km^3) was produced in a period of 21.5 hours or less, and the time-averaged mass discharge rate for the pumice raft is 9 × 10^6 kg s^{-1} (using an average bulk density of rafted pumice clasts of 550 kg m^{-3}; fig. S4).

DISCUSSION

Voluminous deposits dominated by vesicular GP clasts appear to be unique to subaqueous eruptions (*3, 19, 20*). At Havre, we have demonstrated that GP can be produced at high (9 MPa) hydrostatic pressures. The Havre GP deposit footprint is a product of the processes of buoyant rise, water saturation, and distribution by ocean currents. The equant and prismatic shapes and curviplanar surfaces of the GP suggest mechanical detachment of magma extruded into the ocean. The present data suggest that the GP eruption was clast-forming yet not explosive, involving the extrusion of pumiceous rhyolite. Similar to the study of Rotella *et al.* (*10*), we infer that high hydrostatic pressures suppressed bubble expansion in magma. In contrast to the study of Rotella *et al.* (*9*), we favor a model of mechanical or quench release of clasts rather than buoyancy-driven viscous detachment (*19, 20, 23*). The average GP clast density of 550 kg m^{-3} implies that these clasts were temporarily buoyant and then settled from suspension as they saturated. This detachment and dispersal style is unique to subaqueous eruptions. The footprint of the GP deposit (Fig. 2) and stratigraphic and clast fining relationships (fig. S5) strongly suggest that the vent for the GP clasts is beneath dome O-P.

An outstanding question is whether or not there is a relationship between the GP deposit and the pumice raft. Samples from both the interiors and exteriors of GP clasts show distinct macro- and microtextural similarities to raft pumice samples collected from multiple locations (figs. S4 and S6). Modal densities of the GP and raft pumice clasts average between 500 and 600 kg m^{-3}, consistent with those measured by Rotella *et al.* (*10*) (fig. S4). Both are phenocryst-poor (<5% by volume), and phenocrysts are dominated by plagioclase and orthopyroxene. The microlites in both consist of plagioclase and orthopyroxene in varying abundances (table S3). Raft and GP clasts (both interior and exterior) exhibit submillimeter to millimeter textural bands (fig. S6); clasts are predominantly white to pale gray, with dark gray bands that have higher abundances of microlites (table S3). Moreover, the northwest azimuth of the emergent pumice raft (Fig. 1) and the

footprint of the mapped GP deposit on the volcanic edifice (Fig. 2) are coincident, suggesting that both felt similar currents as they traversed the water column. We infer that the seafloor GP deposit comprises clasts that lost buoyancy before joining the raft and settled gently from suspension to the seafloor within 6 km of the source vent. All currently available data are consistent with the GP deposit and the pumice raft having been erupted at roughly the same time from the same source area under dome O-P.

The eruption style that generated the pumice raft has not been resolved. In a subaerial setting, the mass discharge rate (9×10^6 kg s^{-1}) would normally be associated with a magmatic volatile–driven explosive eruption style. Conceptual models of submarine magmatic volatile–driven explosive eruption and transport of pumice (3, 24–26) predict that a range of pyroclast sizes (ALB deposits) will be produced, but that waterlogging and settling times preferentially promote rapid settling of the centimeter-sized lapilli in the proximal environment. At Havre, the proximal GP deposit contains very abundant coarse meter-sized clasts but is impoverished in lapilli (2 to 64 mm in diameter) and ash. If the raft was produced by an explosive eruption driven by magmatic volatiles, the paucity of smaller clasts could imply that the mechanism of submarine magmatic explosivity is fundamentally different from that for subaerial eruptions (9). For example, high hydrostatic pressure may allow magmatic fragmentation to occur at shallow levels in the conduit, limiting the number of energetic particle collisions within the conduit and vent (27), and thereby preserving a population of very coarse pumiceous pyroclasts. More detailed quantitative data, such as the timing and rates of volatile exsolution and magma degassing, need to be established; they will aid in the assessment of the eruption mechanism and allow comparison of the Havre eruption with other proposed submarine eruption styles (3, 10, 28).

If the correlation of the Havre 2012 pumice raft and the GP deposit is correct, then we can estimate the discharge rate of some of the lavas and domes. No differences in morphology of domes H to P were observed between the R/V Tangaroa multibeam (17 October 2012) and the 2015 R/V Revelle multibeam surveys, suggesting that at the time of R/V Tangaroa multibeam survey, these domes were fully emplaced. The GP deposit lies stratigraphically beneath lava domes H to P, so these domes were emplaced after the GP deposit and before the R/V Tangaroa multibeam survey. This stratigraphic constraint gives the maximum duration of lava emplacement of 90 days, assuming that the GP deposit formed on 18 to 19 July 2012. The volumetrically largest dome O-P (0.11 km^3) has a time-averaged effusion rate of >14 m^3 s^{-1} or >3.3 × 10^4 kg s^{-1}, assuming a lava density of 2350 kg m^{-3} (table S2). These rates are minima as most of the O-P dome growth could have been completed within a shorter time interval. These time-averaged effusion rates are equal to those of comparable subaerial silicic examples, such as Mount St. Helens in October to December 1980 (3 to 13 m^3 s^{-1}) (29) and Puyehue volcano in 2011 (17 m^3 s^{-1}) (30), but less than that of Chaitén volcano in 2008 (45 m^3 s^{-1}) (31).

At Havre, the satellite-based record of the pumice raft and the detailed submarine survey permit us to calculate mass partitioning of pumice clasts into proximal versus rafted and hence distal environments. Our volume estimates reveal that most of the erupted volume (>75%) was transported away from the volcanic edifice (32). This percentage is comparable to that of similar magnitude subaerial fall deposits (33). However, unlike subaerial fall deposits where exponential and power law relationships between deposit thickness and distance can be used to calculate mass partitioning and total mass erupted (34), there are no models for marine dispersal that incorporate water depth,

duration of particle buoyancy, ocean stratification, current speed and direction, or sea-surface wind shear, all of which are necessary for prediction of marine dispersal. There is no direct evidence on Havre of the eruption that produced the raft, the most voluminous product of the 2012 eruption. Consequently, for similar events, submarine eruption size cannot be reconstructed accurately from seafloor or uplifted deposits; this lost information is a source of uncertainty when assessing magma productivity in submarine volcanic arcs.

MATERIALS AND METHODS
Calculation of pumice raft areas, timing of generation, and raft volumes
Terra and Aqua satellites capture moderate-resolution (250 m/pixel) images twice daily using the MODIS instrument. At the location and month of the eruption, photo intervals were timed every ca. 3.5- and 21-hour intervals. We observed the first appearance of a raft in the water on 18 July at about 00:45 UTC to the southeast of the Havre submarine caldera. The next image (21:51 UTC, 18 July) showed that the pumice raft rapidly grew into a uniform area of ~210 km^2 that was likely to have still been connected to its point source. On the morning of 19 July (01:26 UTC; 24 hours and 41 min from the observed first appearance), the main raft was 400 km^2 and was slightly disconnected from its point source. On the basis of water currents and the position of the first raft appearance, we calculated the first appearance of the raft at ca. 22:00 UTC on 17 July. Similarly, on the basis of the distance of the disconnected raft and water current velocity, we estimated that the raft separated from the point source 6 hours before the 01:26 UTC MODIS image (18 July, 19:30 UTC). Our estimated duration of the main raft formation was thus 21.5 hours.

Jutzeler et al. (16) documented an absolute minimum bulk volume of the 400-km^2 pumice raft to be 0.11 to 0.16 km^3 based on a minimum raft thickness of 50 to 70 cm at a clast packing density of 60%. We modify that volume assessment with the following constraints:

(1) Three weeks after the eruption, a navy ship encountered the raft (21). Clasts with a diameter of 75 cm were collected, and the raft was densely packed and at least two clasts thick.

(2) The raft was stable and highly reflective for the 24 hours constrained in satellite imagery (three images). This stability and reflectivity suggest sustained and dense packing of the raft. Dense packing of pumice rafts has been documented previously. Observations of the early pumice rafts from the 1883 Krakatoa eruption described multiple-clasts-thick rafts that could sustain the weight of men walking on them (35), attesting to the dense packing of the rafts.

The new assessment and calculations of raft volume considered the 400-km^2 raft to contain meter-sized pumice clasts that were two to three clasts thick such that the raft thickness was ~5 m at a clast packing density of 60%. We considered these estimates as minima because the adjacent curtains of submerged pumice clasts and fine particles (in aqua color in fig. S1) and deeper (<200m) submerged pumices/pumice clasts were not incorporated into our estimate. As an indication of the error associated with the thickness estimate, bulk volumes assuming raft thicknesses of 2 and 10 m and a packing density of 60% were 0.48 and 2.4 km^3, respectively.

Calculation of seafloor product volumes
Volume: Seafloor lavas
The volumes of proximal lava flows and domes were determined by comparing the newly acquired AUV Sentry bathymetric maps with

pre-eruption ship-based bathymetric maps collected by the National Institute of Water and Atmospheric Research (NIWA). The difference in the resolution of the two maps (1 m/pixel versus 25 m/pixel) resulted in some uncertainty in the volumes but was more accurate than a comparison of ship-based bathymetric maps. Our volume estimates were calculated only within the boundaries of lavas and domes where we had high confidence of newly deposited products based on landforms imaged in the *Sentry* bathymetry. Outside of these areas, we found the depth differences to have a median of ~6 m. The depth differences showed greater variance along the caldera walls. This result was consistent with ship-based bathymetry smearing high-relief features and with slight mismatches in navigation. On the caldera floor, the delta depth was positive, with a median of ~10 m, although this did not differ greatly from delta depth in areas outside of the footprint of the GP deposit (~5 m) or the overall survey (~6 m). This small difference between the caldera floor and unaffected areas was consistent with the accumulation of GP. However, the data also suggested a small bias toward positive depth differences throughout the survey and limited our confidence in detecting features with less than 10 m of new relief (+/−).

Single lava volumes are given in table S2. Volumes of pyroclastic deposits are determined as follows: proximal GP deposit (bulk), 35 $km^2 \times$ 5 m average thickness × 60% packing = 0.1 km^3; ALB deposit (bulk), cone with a radius of 2 km and a maximum height of 2 m = $\pi r^2(h/3) \times$ 60% packing = 0.005 km^3; AL deposit (bulk), 20 cm average deposit thickness over 35 km^2, with 90% clast packing = 0.063 km^3 (deposit is predominantly ash, and therefore, packing density is increased to 90%).

SUPPLEMENTARY MATERIALS

Supplementary material for this article is available at http://advances.sciencemag.org/cgi/content/full/4/1/e1701121/DC1

fig. S1. MODIS Terra and Aqua satellite images of the region around Havre volcano collected between 18 and 19 July 2012 (UTC).
fig. S2.1. AUV high-resolution bathymetry of Havre submarine volcano.
fig. S2.2. Dive tracks for the AUV *Sentry*.
fig. S2.3. ROV track lines.
fig. S3. Detailed views of seafloor roughness.
fig. S4. Clast density distributions from Havre and other Kermadec volcanoes.
fig. S5. GP size with distance.
fig. S6. Clast textures from seafloor GP and raft pumice.
movie S1. GP retrieval from the seafloor.
table S1A. X-ray fluorescence geochemical data of 2012 products.
table S1B. X-ray fluorescence geochemical precision and accuracy data.
table S2. Table of Havre lava volumes.
table S3. Phenocryst assemblages and microlite populations of the GP and raft pumice from petrographic analysis.
References (*35–37*)

REFERENCES AND NOTES

1. J. A. Crisp, Rates of magma emplacement and volcanic output. *J. Volcanol. Geotherm. Res.* **20**, 177–211 (1984).
2. J. D. L. White, C. I. Schipper, K. Kano, Submarine explosive eruptions, in *The Encyclopedia of Volcanoes*, H. Sigurdsson, B. Houghton, S. R. McNutt, H. Rymer, J. Stix, Eds. (Academic Press, ed. 2, 2015), pp. 553–569.
3. S. R. Allen, J. McPhie, Products of neptunian eruptions. *Geology* **37**, 639–642 (2009).
4. R. W. Embley, W. W. Chadwick Jr., E. T. Baker, D. A. Butterfield, J. A. Resing, C. E. J. de Ronde, V. Tunnicliffe, J. E. Lupton, S. K. Juniper, K. H. Rubin, R. J. Stern, G. T. Lebon, K.-i. Nakamura, S. G. Merle, J. R. Hein, D. A. Wiens, Y. Tamura, Long-term eruptive activity at a submarine arc volcano. *Nature* **441**, 494–497 (2006).
5. J. A. Resing, K. H. Rubin, R. W. Embley, J. E. Lupton, E. T. Baker, R. P. Dziak, T. Baumberger, M. D. Lilley, J. A. Huber, T. M. Shank, D. A. Butterfield, D. A. Clague, N. S. Keller, S. G. Merle, N. J. Buck, P. J. Michael, A. Soule, D. W. Caress, S. L. Walker, R. Davis, J. P. Cowen, A.-L. Reysenbach, H. Thomas, Active submarine eruption of boninite in the northeastern Lau Basin. *Nat. Geosci.* **4**, 799–806 (2011).
6. N. D. Deardorff, K. V. Cashman, W. W. Chadwick Jr., Observations of eruptive plume dynamics and pyroclastic deposits from submarine explosive eruptions at NW Rota-1, Mariana arc. *J. Volcanol. Geotherm. Res.* **202**, 47–59 (2011).
7. K. Kano, Subaqueous pumice eruptions and their products; a review, in *Explosive Subaqueous Volcanism*, J. D. L. White, J. L. Smellie, D. A. Clague, Eds. (American Geophysical Union, 2003), vol. 140, pp. 213–229.
8. R. S. Fiske, J. Naka, K. Iizasa, M. Yuasa, A. Klaus, Submarine silicic caldera at the front of the Izu-Bonin arc, Japan; voluminous seafloor eruptions of rhyolite pumice. *Geol. Soc. Am. Bull.* **113**, 813–824 (2001).
9. M. D. Rotella, C. J. N. Wilson, S. J. Barker, I. C. Wright, Highly vesicular pumice generated by buoyant detachment of magma in subaqueous volcanism. *Nat. Geosci.* **6**, 129–132 (2013).
10. M. D. Rotella, C. J. N. Wilson, S. J. Barker, C. I. Schipper, I. C. Wright, R. J. Wysoczanski, Dynamics of deep submarine silicic explosive eruptions in the Kermadec arc, as reflected in pumice vesicularity textures. *J. Volcanol. Geotherm. Res.* **301**, 314–332 (2015).
11. I. C. Wright, J. A. Gamble, P. A. Shane, Submarine silicic volcanism of the Healy caldera, southern Kermadec arc (SW Pacific): I—Volcanology and eruption mechanisms. *Bull. Volcanol.* **65**, 15–29 (2003).
12. M. A. Reynolds, J. G. Best, Summary of the 1953–57 eruption of Tuluman volcano, Papua New Guinea, in *Volcanism in Australasia*, R. W. Johnson, Ed. (Elsevier, 1976), pp. 287–296.
13. M. A. Reynolds, J. G. Best, R. W. Johnson, *1953–57 Eruption of Tuluman Volcano: Rhyolitic Volcanic Activity in the Northern Bismarck Sea (Memoir/Geological Survey of Papua New Guinea)* (Geological Survey of Papua New Guinea, 1980), vol. 7, p. 44.
14. R. S. Fiske, K. V. Cashman, A. Shibata, K. Watanabe, Tephra dispersal from Myojinsho, Japan, during its shallow submarine eruption of 1952–1953. *Bull. Volcanol.* **59**, 262–275 (1998).
15. F. Maeno, H. Taniguchi, Silicic lava dome growth in the 1934–1935 Showa Iwo-jima eruption, Kikai caldera, south of Kyushu, Japan. *Bull. Volcanol.* **68**, 673–688 (2006).
16. M. Jutzeler, R. Marsh, R. J. Carey, J. D. L. White, P. J. Talling, L. Karlstrom, On the fate of pumice rafts formed during the 2012 Havre submarine eruption. *Nat. Commun.* **5**, 3660 (2014).
17. R. J. Carey, R. Wysoczanski, R. Wunderman, M. Jutzeler, Discovery of the largest historic silicic submarine eruption. *Eos Trans. AGU* **95**, 157–159 (2014).
18. I. C. Wright, T. J. Worthington, J. A. Gamble, New multibeam mapping and geochemistry of the 30°–35° S sector, and overview, of southern Kermadec arc volcanism. *J. Volcanol. Geotherm. Res.* **149**, 263–296 (2006).
19. S. R. Allen, J. McPhie, Water-settling and resedimentation of submarine rhyolitic pumice at Yali, eastern Aegean, Greece. *J. Volcanol. Geotherm. Res.* **95**, 285–307 (2000).
20. S. R. Allen, R. S. Fiske, Y. Tamura, Effects of water depth on pumice formation in submarine domes at Sumisu, Izu-Bonin Arc, western Pacific. *Geology* **38**, 391–394 (2010).
21. H. Bostock, "Pumice raft observations at Havre" (New Zealand Institute of Water and Atmospheric Research Internal Report, NIWA, Wellington, 2012).
22. G. P. L. Walker, New Zealand case histories of pyroclastic studies, in *Tephra Studies*, S. Self, R. S. J. Sparks, Eds. (D. Reidel Publishing Company, 1981), pp. 317–330.
23. I. J. von Lichtan, J. D. L. White, V. Manville, C. Ohneiser, Giant rafted pumice blocks from the most recent eruption of Taupo volcano, New Zealand: Insights from palaeomagnetic and textural data. *J. Volcanol. Geotherm. Res.* **318**, 73–88 (2016).
24. K. V. Cashman, R. S. Fiske, Fallout of pyroclastic debris from submarine volcanic eruptions. *Science* **253**, 275–280 (1991).
25. V. Manville, J. D. L. White, B. F. Houghton, C. J. N. Wilson, The saturation behaviour of pumice and some sedimentological implications. *Sediment. Geol.* **119**, 5–16 (1998).
26. S. R. Allen, R. S. Fiske, K. V. Cashman, Quenching of steam-charged pumice: Implications for submarine pyroclastic volcanism. *Earth Planet. Sci. Lett.* **274**, 40–49 (2008).
27. J. Dufek, M. Manga, A. Patel, Granular disruption during explosive volcanic eruptions. *Nat. Geosci.* **5**, 561–564 (2012).
28. K. Kano, A Miocene coarse volcaniclastic mass-flow deposit in the Shimane Peninsula, SW Japan: Product of a deep submarine eruption? *Bull. Volcanol.* **58**, 131–143 (1996).
29. S. W. Anderson, J. H. Fink, W. I. Rose, Mount St. Helens and Santiaguito lava domes: The effect of short-term eruption rate on surface texture and degassing processes. *J. Volcanol. Geotherm. Res.* **69**, 105–116 (1995).
30. D. Bertin, L. E. Lara, D. Basualto, Á. Amigo, C. Cardona, L. Franco, F. Gil, J. Lazo, High effusion rates of the Cordón Caulle 2011–2012 eruption (Southern Andes) and their relation with the quasi-harmonic tremor. *Geophys. Res. Lett.* **42**, 7054–7063 (2015).
31. J. S. Pallister, A. K. Diefenbach, W. C. Burton, J. Muñoz, J. P. Griswold, L. E. Lara, J. B. Lowenstern, C. E. Valenzuela, The Chaitén rhyolite lava dome: Eruption sequence, lava dome volumes, rapid effusion rates and source of the rhyolite magma. *Andean Geol.* **40**, 277–294 (2013).
32. K. Tani, R. S. Fiske, Y. Tamura, Y. Kido, J. Naka, H. Shukuno, R. Takeuchi, Sumisu volcano, Izu-Bonin arc, Japan: Site of a silicic caldera-forming eruption from a small open-ocean island. *Bull. Volcanol.* **70**, 547–562 (2008).

33. D. M. Pyle, The thickness, volume and grainsize of tephra fall deposits. *Bull. Volcanol.* **51**, 1–15 (1989).

34. C. Bonadonna, A. Costa, Modeling of tephra sedimentation from volcanic plumes, in *Modeling Volcanic Processes: The Physics and Mathematics of Volcanism* (Cambridge Univ. Press, 2013), pp. 173–202.

35. T. Simkin, R. S. Fiske, Krakatau 1883. *Earthquake Inf. Bull.* **15**, 128–133 (1983).

36. B. F. Houghton, C. J. N. Wilson, A vesicularity index for pyroclastic deposits. *Bull. Volcanol.* **51**, 451–462 (1989).

37. S. J. Barker, M. D. Rotella, C. J. N. Wilson, I. C. Wright, R. J. Wysoczanski, Contrasting pyroclast density spectra from subaerial and submarine silicic eruptions in the Kermadec arc: Implications for eruption processes and dredge sampling. *Bull. Volcanol.* **74**, 1425–1443 (2012).

Citation: R. Carey, S. A. Soule, M. Manga, J. D. L. White, J. McPhie, R. Wysoczanski, M. Jutzeler, K. Tani, D. Yoerger, D. Fornari, F. Caratori-Tontini, B. Houghton, S. Mitchell, F. Ikegami, C. Conway, A. Murch, K. Fauria, M. Jones, R. Cahalan, W. McKenzie, The largest deep-ocean silicic volcanic eruption of the past century. *Sci. Adv.* **4**, e1701121 (2018).

The largest deep-ocean silicic volcanic eruption of the past century

Rebecca Carey, S. Adam Soule, Michael Manga, James D. L. White, Jocelyn McPhie, Richard Wysoczanski, Martin Jutzeler, Kenichiro Tani, Dana Yoerger, Daniel Fornari, Fabio Caratori-Tontini, Bruce Houghton, Samuel Mitchell, Fumihiko Ikegami, Chris Conway, Arran Murch, Kristen Fauria, Meghan Jones, Ryan Cahalan and Warren McKenzie

ARTICLE TOOLS	http://advances.sciencemag.org/content/4/1/e1701121
SUPPLEMENTARY MATERIALS	http://advances.sciencemag.org/content/suppl/2018/01/08/4.1.e1701121.DC1
REFERENCES	This article cites 30 articles, 4 of which you can access for free http://advances.sciencemag.org/content/4/1/e1701121#BIBL
PERMISSIONS	http://www.sciencemag.org/help/reprints-and-permissions